

## SOLID SOLUBILITY IN Cu<sub>5</sub>Gd<sub>1-x</sub>Ca<sub>x</sub> SYSTEM: STRUCTURE, STABILITY, HYDROGENATION AND CATALYSIS OF OXYGEN REDUCTION

Andraž Kocjan<sup>1</sup>, Luka Kelhar<sup>1,4</sup>, Anton Gradišek<sup>1</sup>, Blaž Likozar<sup>2</sup>,  
Kristina Žagar<sup>1,4</sup>, Spomenka Kobe<sup>1,4\*</sup>, Jean-Marie Dubois<sup>3,4</sup>

<sup>1</sup> Jožef Stefan Institute, Jamova cesta 39, SI-1000 Ljubljana, Slovenia

<sup>2</sup> National Institute for Chemistry, Hajdrihova ulica 19, SI-1000 Ljubljana, Slovenia

<sup>3</sup> Institut Jean Lamour (UMR 7198 CNRS-Université de Lorraine), Parc de Saurupt, CS50840, 54011 Nancy Cedex, France

<sup>4</sup> PACS2 International Associated Laboratory CNRS-Jožef Stefan Institute, Nancy and Ljubljana, Slovenia

**Abstract:** We studied the effects of substituting gadolinium in the compound Cu<sub>5</sub>Gd with Ca by investigating the phase stability and crystal structure of the resulting new compounds. For rapidly quenched materials produced by melt spinning, the crystal structure was always hexagonal P<sub>6</sub>/mmm, irrespective of the Ca addition (*x*) in alloys with the formula Cu<sub>5</sub>Gd<sub>1-x</sub>Ca<sub>x</sub>, indicating good solid solubility under these conditions, which was additionally confirmed by Vegard's law. Slower cooling upon arc-melting process caused the phase separation into Cu<sub>4</sub>Gd and CuCa. Using TEM, we investigated rapidly solidified ribbons of Cu<sub>5</sub>Gd<sub>0.5</sub>Ca<sub>0.5</sub> and observed co-existence of Cu–Ca secondary phase with a matrix phase having the nominal stoichiometric composition. The oxygen level in this sample was found to be within 2–5 at. %, which was attributed to surface oxidation during or after TEM sample preparation. Upon hydrogenation, the crystal structure of all samples changed from hexagonal to cubic (F-43m), which is the thermodynamically stable polymorph of Cu<sub>5</sub>Gd compound. Strong catalytic activity of water formation from gaseous H<sub>2</sub> and O<sub>2</sub> was coincidentally discovered during dehydrogenation experiment, thus making this material as potential candidate for zero-platinum oxygen reduction catalyst.

**Keywords:** rapid solidification, solid solubility, phase transition, hydrogenation, catalysis.

### 1. INTRODUCTION

A number of empirical rules based on the thermodynamic criteria have been developed to predict the formation of solid solutions in metallic systems. Hume-Rothery rules [1] have been used for decades in the traditional alloying design, as they postulate the conditions for substitutional solid solubility in binary systems, i.e. same crystal structure and valence state, similar electronegativity and the difference in atom size between solute and solvent should be less than 15 %. However, for alloys with more than two constituent elements, especially for so-called high entropy alloys (HEA), which contain five or more elements in equi-molar ratio, other rules and parameters must be applied, as reported by Takeuchi and Inoue [2], Zhang et al. [3] and Guo et al. [4,5]. These authors derived the following criteria, which can be applied for phase selection and

stability in multi-element metallic systems: atomic size mismatch ( $\delta$ ), electronegativity difference ( $\Delta\chi$ ), valence electron concentration (VEC or  $e/a$ ) and enthalpy of mixing ( $\Delta H_{\text{mix}}$ ).

Nevertheless, all authors agree that the mixing enthalpy and atomic size mismatch parameters are detrimental for the formation of specific phase, i.e. either intermetallic, solid solution or amorphous. Guo et al. [5] proposed a plot of  $\Delta H_{\text{mix}}$  and  $\delta$  for different multi-element alloys, which shows that the solid solution area is within the range  $-12 \text{ kJ/mol} < \Delta H_{\text{mix}} < 10 \text{ kJ/mol}$  and  $0 < \delta < 6.6 \%$ . As the mixing enthalpy is getting more negative and atomic radii mismatch larger than previously mentioned value, then intermetallic and amorphous phases start to form. Another condition must be fulfilled in order for solid solution to form, seen from Eq. 1, known as Gibbs free energy of mixing. Namely, the first term,  $\Delta H_{\text{mix}}$ , should ideally be around zero,

\* Corresponding author: spomenka.kobe@ijs.si

whereas the entropy term,  $T\Delta S_{\text{mix}}$ , should be larger than the enthalpy term.

$$\Delta G_{\text{mix}} = \Delta H_{\text{mix}} - T\Delta S_{\text{mix}} \quad (1)$$

The entropy of mixing is related to the statistical-mechanics definition of entropy developed by Ludwig Boltzmann in the 1870s [6], who stated that the entropy of a system is linearly proportional to the natural logarithm of the frequency of occurrence or possible configurations ( $W$ ), Eq. 2, also known as the configurational entropy:

$$S = k \ln W \quad (2)$$

where  $k = 1.38 \times 10^{-23}$  J/K is the Boltzmann's constant. The configurational entropy of mixing with  $N$  components can be derived for a random solid solution as:

$$\Delta S_{\text{mix}} = -R \sum_{i=1}^N c_i \ln c_i \quad (3)$$

where  $R = 8.31$  J/mol K is the gas constant, and  $c_i$  is the molar fraction of the  $i$ th component. Thus, the entropy of mixing increases with the number of elements in the alloy, and reaches the maximum at the equi-molar ratio. For most common HEAs based on Cr, Fe, Co and Ni, this means, that when the alloy consists of 5 or more elements,  $T\Delta S_{\text{mix}}$  term from Eq. 1 is much larger than  $\Delta H_{\text{mix}}$  at the melting point, thus slow solidification is sufficient to obtain solid solution. It should be emphasized, that the mixing enthalpies of previously mentioned transition metals are all close to zero, which enables ideal mixing and therefore high solid solubility even at low number of elements. However, when  $\Delta H_{\text{mix}}$  is too negative, then intermetallic phases will form, if too positive, segregation of certain element or strong phase separation will occur at slow or moderate cooling rate. Therefore, rapid solidification, i.e. melt-spinning, must be applied in such cases in order to obtain single (solid-solution) phase, especially when the configurational entropy is low, i.e. in ternary systems.

The entropy of fusion, which is the increase in entropy when melting a substance, additionally improves solid-solution-formability. This value is always positive, since the degree of disorder increases from a long-range-ordered solid to a disordered structure of a liquid [7]. The entropy of fusion is denoted as  $\Delta S_f$  and normally expressed in J/mol K. A natural process, such as a phase change, will occur when the associated change in the Gibbs free energy is negative. It follows that the entropy of fusion is related to the melting point and the heat of fusion:

$$\Delta S_f = \frac{\Delta H_f}{T_f} \quad (4)$$

where  $\Delta H_f$  is the heat of fusion or the latent heat of fusion, and  $T_f$  is the melting point. However, for the pure metal or the pure substance,  $T_f$  is one point, while for the alloys, there is a temperature range,

except for those alloys that involve invariant reactions, such as the congruent melting or eutectic point: the solidus temperature ( $T_s$ ) at which the melting starts, the liquidus temperature ( $T_L$ ) at which melting finishes. In between the two temperatures, the alloy is in a state of mixture of solid and liquid phases. For pure metals or traditional binary metallic alloys, the fusion entropy is around 1R [8], whereas the entropy of mixing for a ternary equi-molar ratio element alloy is usually higher than that of the fusion entropy, and the difference between them becomes even larger for the higher-order HEAs.

In our study, we have focused on ternary Cu-Gd-Ca system, which has not been reported in the literature so far, although the first reports on the Cu-Gd [9–11] and Cu-Ca [12,13] systems go back in the 1980s. Therefore, we found it challenging to search for new ternary compounds in the Cu-Gd-Ca system, where the primary goal was to discover new quasicrystals. Namely, there is more than 99.6 % miscibility gap for the elements Ca and Gd, which means that they form neither stable compound, nor solid solution. Even more, up to date no phase diagram is available for Gd-Ca system. Immiscibility in the liquid phase has been observed by Kato [14] and Gschneider [15]. However, when a third element is added, the one that forms stable binary phases with both immiscible elements, then new ternary intermetallic phases should form, where some of these might have a complex or even aperiodic structure. A good example of such phenomenon is the Al-Cu-Fe system [16], where copper and iron are completely immiscible, whereas aluminum reacts with both elements individually. When all three elements are combined, many intermetallic compounds, including stable icosahedral quasicrystals, are formed.

Up to date we discovered no quasicrystals or complex structures in Cu-Gd-Ca system. Instead, strong solid solubility of Cu<sub>5</sub>Gd and Cu<sub>5</sub>Ca compounds was observed, though only through rapid quenching. Thus, in this paper we report on the synthesis, structure and stability of Cu<sub>5</sub>Gd<sub>1-x</sub>Ca<sub>x</sub> ( $x = 0, 0.33, 0.5, 0.66, 1$ ) system. We also provide the results of loading the samples with hydrogen, which changes the crystal structure. At the end, we discuss a peculiar catalytic effect of these hydride samples on oxygen reduction, namely water formation from hydrogen and oxygen gasses, which makes this alloy system a potential candidate for zero-platinum oxygen reduction catalyst in hydrogen (PEM) fuel cells. Specifically, Gd-promoted oxygen reduction catalyst were predominantly examined recently preparing materials, containing noble metals such as platinum [17–19], however completely avoiding the latter is definitely of interest, although further tests including long-term stability are needed as ultimate benchmark.

## 2. EXPERIMENTAL

The experimental study investigated five samples with the general formula Cu<sub>5</sub>Gd<sub>1-x</sub>Ca<sub>x</sub> ( $x = 0, 0.33, 0.5, 0.66$  and  $1$ ), which were prepared by arc-melting and melt-spinning in high-purity (99.9999 %) argon gas. First, copper and gadolinium pieces were arc-melted to form a eutectic, since calcium is extremely volatile. The arc-melted precursors were then spun on the rotating copper wheel at 40 m/s using boron-nitride-coated graphite crucibles to prevent the formation of any carbide phases in the ribbons. In order to minimize the Ca evaporation we increased the pressure in the melt-spinning chamber from the standard 700 mbar to 1500 mbar. In spite of this, 2–3 wt. % of excess Ca had to be added to maintain the stoichiometry. The X-ray diffraction (XRD) patterns were recorded using a PANalytical diffractometer with Cu-K $\alpha$  radiation in the  $2\Theta$  interval 2–60°. Hydrogenation was performed under 1 bar of 99.999 % hydrogen gas at 300°C for 16 hours. The heating rate at high-temperature XRD experiment was 20°min<sup>-1</sup>, whereas the set temperatures were 400, 580 and 700°C. For the DSC analysis the temperature scheme was as follows: 20°min<sup>-1</sup> to 800°C, natural cooling to 200°C and then 20°min<sup>-1</sup> to 800°C. TEM investigation was performed by Jeol JEM ARM 200 CF microscope. The sample preparation included mechanical grinding and dimpling using isopropanol to avoid oxidation, and subsequent Ar ion-milling. Gas Analytical System QMS 403 C Aëolos (STA 449 C/6/G Jupiter® - QMS

403 C, Netzsch, Germany) thermal analyzer with an attached mass spectrometer were used to perform DSC and mass-spectrometry of desorbed hydrogen from hydrogenated samples by 20°min<sup>-1</sup> heating up to 800°C. For catalytic activity tests under controlled atmosphere, the samples were subjected to model reaction system using the Micromeritics AutoChem II Chemisorption Analyzer apparatus, employing thermal conductivity detector (TCD) to determine the H<sub>2</sub> consumption/evolution. Firstly, they were heated from 25°C to 200°C using a heating rate of 10°min<sup>-1</sup> at constant O<sub>2</sub> in He (1 %) flow rate (100 mL/min) and then they were maintained at the final temperature for 20 min. Mass spectrometry (MS) (ThermoStar, Pfeiffer Vacuum) was used to determine the amount of the reactants and products in effluent gases (maintained at 130 °C) by monitoring the characteristic  $m/z$  signals for H<sub>2</sub>O ( $m/z = 18.00$ ) and O<sub>2</sub> ( $m/z = 32.00$ ). Afterwards, the samples were cooled in He (6.0) and subjected in turn to the same program, with the only difference of using O<sub>2</sub>/H<sub>2</sub> in He/Ar (2/4 % in 18/76 %) over the prepared materials.

## 3. RESULTS AND DISCUSSION

The compositions of the prepared samples were plotted on a partial Cu-Gd-Ca ternary phase diagram in Figure 1, i.e. Cu<sub>5</sub>Gd<sub>1-x</sub>Ca<sub>x</sub> ( $x = 0, 0.33, 0.5, 0.66$  and  $1$ ).

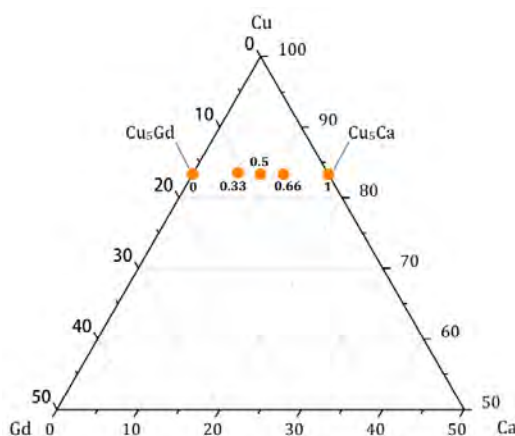


Figure 1. The Cu-rich half of the Cu–Gd–Ca ternary phase diagram with the marked Cu<sub>5</sub>Gd<sub>1-x</sub>Ca<sub>x</sub> compositions, where  $x$  values are given at each corresponding point

### Microstructure

Figure 2a shows a microstructure of the arc-melted Cu<sub>5</sub>Gd<sub>0.5</sub>Ca<sub>0.5</sub> sample. There is clear evidence for a strong phase separation at slow cooling, since even after addition of the third element, copper, to immiscible Gd-Ca system, these two elements do not coexist in a single phase, but rather form binary

phases with copper, instead. The bright phase is Cu<sub>4</sub>Gd, whereas dark phase is the equi-atomic CuCa compound. It must be noted that Cu<sub>4</sub>Gd compound does not exist in Cu-Gd phase diagram, as reported by [9–11]. However, these authors report on Cu<sub>9</sub>Gd<sub>2</sub> compound, which is the closest to Cu<sub>4</sub>Gd composition that we observed.

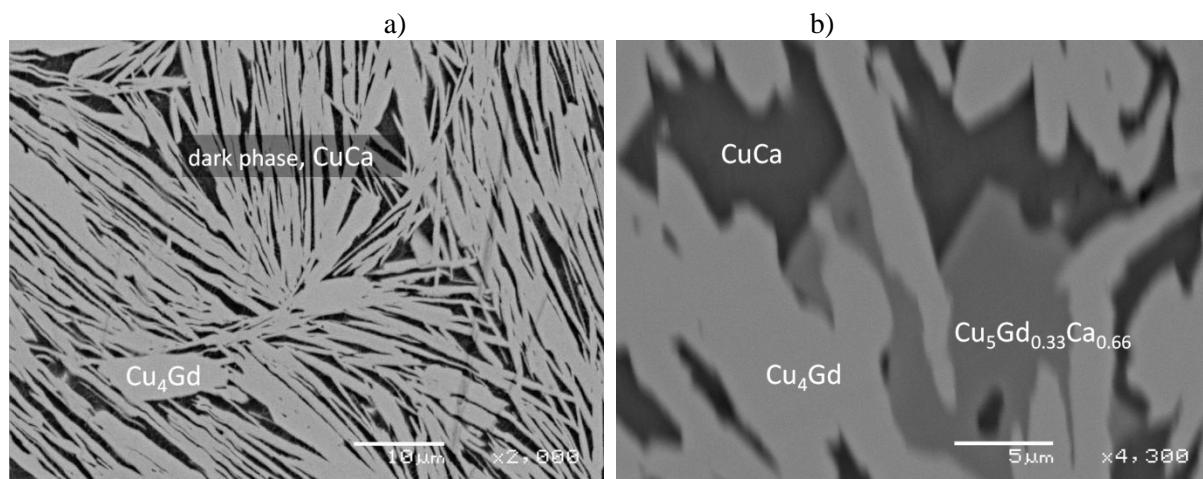


Figure 2. SEM z-contrast images of polished surface of a) arc-melted  $\text{Cu}_5\text{Gd}_{0.5}\text{Ca}_{0.5}$  sample, and b) the same sample after 7 days of homogenization at 700 °C in an argon-filled, sealed silica tube and subsequently ice-water quenched

The difference in Cu amount between these two compounds is almost 2 at. %, which we believe is too large to be attributed to EDS experimental error that is estimated around  $\pm 0.5$  at. %. Especially, because the series of EDS data that we observed on several arc-melted samples were very repeatable for  $\text{Cu}_4\text{Gd}$  bright phase. Therefore we concluded, that  $\text{Cu}_4\text{Gd}$  phase is a new compound, not reported before. If Ca addition and consequent phase separation, forming CuCa phase, is essential for  $\text{Cu}_4\text{Gd}$  formation, was not the subject of further investigation.

In an attempt to produce the very first ternary phase of this system, we homogenized the arc-melted button in a sealed silica tube containing Ti-getter under highly pure argon gas at 700°C for 7 days, and subsequently ice-water quenched. An SEM z-contrast image with the associated EDS analyses are shown in Figure 2b. Beside the bright  $\text{Cu}_4\text{Gd}$  phase, we observed ~1 at. % of Gd dissolved in a dark CuCa phase and, more importantly, a new ternary intermetallic compound with an intermediate z-contrast with composition  $\text{Cu}_5\text{Gd}_{0.33}\text{Ca}_{0.66}$  was found. To the best of our knowledge, up to date this is the first report of any Cu-Gd-Ca intermetallic compound. Thus, in order to obtain a single phase  $\text{Cu}_5\text{Gd}_{0.33}\text{Ca}_{0.66}$  sample, we used rapid quenching technique, i.e. melt-spinning, for its preparation. This method was proved successful, since back-scattered SEM imaging and EDS analysis revealed a single phase material with nominal stoichiometric composition. The same results were obtained for other four samples.

We performed a TEM characterization of  $x=0.5$  as-spun sample, Figure 3, in order to check whether the melt-spun ribbons were completely homogeneous, which cannot be determined by XRD, since the coexisting phases might have an identical

structure, nor by SEM, due to the limited resolution of EDS probe. Cu-Ca secondary phase was found to coexist in the matrix phase that had a stoichiometric  $\text{Cu}_5\text{Gd}_{0.5}\text{Ca}_{0.5}$  composition. Using SAED, we confirmed the hexagonal structure of the matrix phase, which is in agreement with the XRD results. Since no additional XRD peaks were found, we could conclude that the Cu-Ca secondary phase had the same crystal structure as the stoichiometric matrix phase. The estimated population of secondary phase was around 10 vol. %, which was enough to be seen by XRD, in case it would have different structure.

The amount of oxygen detected in the matrix phase was 2 at. %, while in the Cu-Ca secondary phase it was 5 at. %, which both can be attributed to surface oxidation during or after TEM sample preparation.

#### X-ray diffraction

XRD patterns of the as-spun ribbons in Figure 4 indicate good solid solubility of the copper, gadolinium and calcium in the  $\text{Cu}_5\text{Gd}_{1-x}\text{Ca}_x$  system due to the preservation of the hexagonal structure as the Gd is substituted with increasing amounts of Ca ( $x$ ). It is clear that the rapid cooling rates associated with melt-spinning are vital for the preparation of a single-phase material. There was slight variation of peak positions in the XRD patterns, as well as some differences in the relative intensities were found, particularly for the 010 peak. The first could be attributed to the lattice parameters modification, whereas the second to the structure factor, i.e. different positions of the atoms within the  $P_6/mmm$  unit cell. Experimental data revealed 1.6 % difference between  $\text{Cu}_5\text{Gd}$  and  $\text{Cu}_5\text{Ca}$  unit cell volumes.

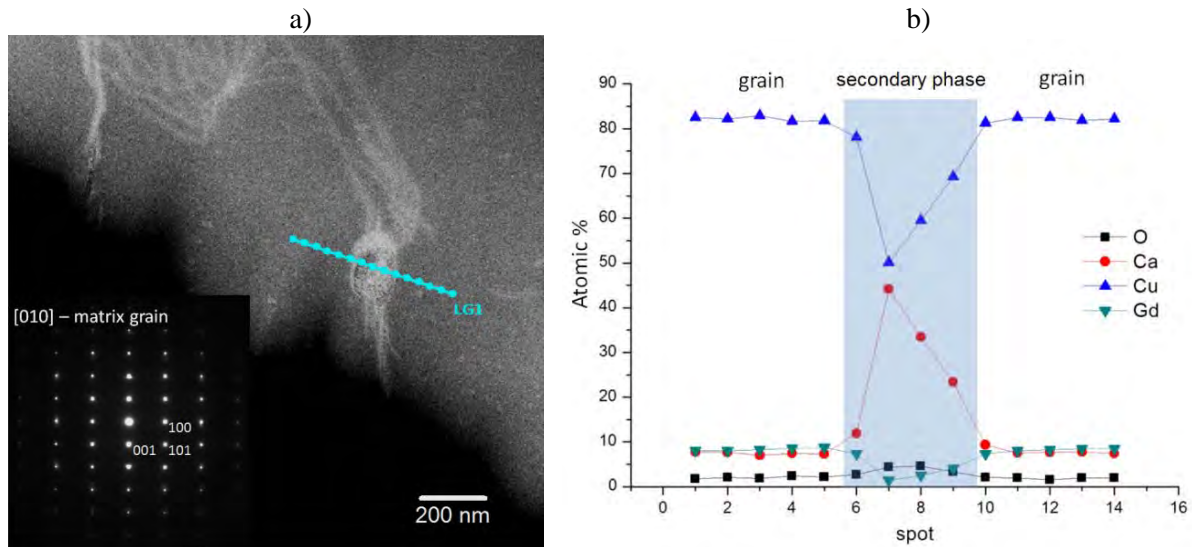


Figure 3. a) Cross-section TEM image of a  $\text{Cu}_5\text{Gd}_{0.5}\text{Ca}_{0.5}$  melt-spun ribbon shows that matrix grains have hexagonal symmetry (SAED). In addition, about 10 % of randomly distributed secondary Cu-Ca phase was found; b) EDS line scan (14 points) confirmed stoichiometric, i.e. nominal, composition of the matrix phase, low oxygen level and segregation of Cu-Ca phase

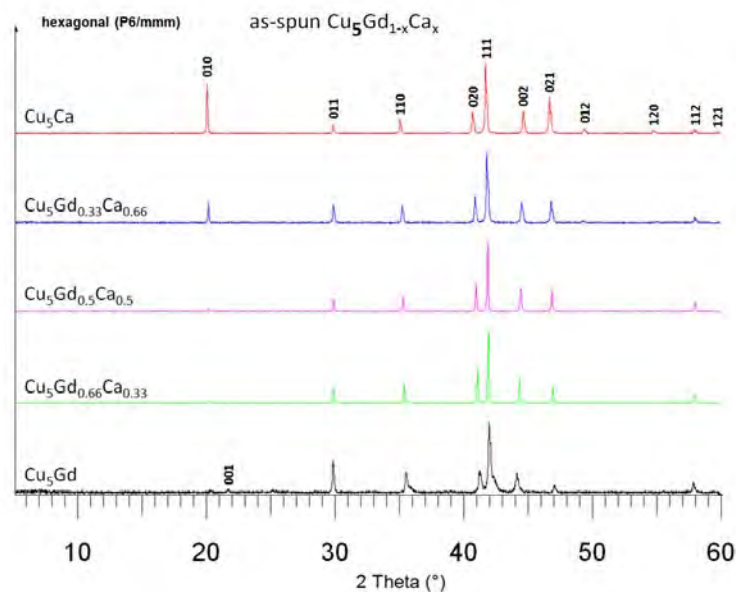


Figure 4. XRD patterns of  $\text{Cu}_5\text{Gd}_{1-x}\text{Ca}_x$  ( $x = 0, 0.33, 0.5, 0.66$  and  $1$ ) ribbons, melt-spun at  $40 \text{ m/s}$

When describing the dependence of lattice parameters and compositional factor  $x$ , we used the so-called Vegard's law [20], which is an approximate empirical rule, which holds that a linear relation exists, at constant temperature, between the crystal lattice parameters of a solid solution and the concentrations of the constituent elements (or binary compounds). In case of  $\text{Cu}_5\text{Gd}_{1-x}\text{Ca}_x$  ternary system, such relation can be written as Eq. 5:

$$a(\text{Cu}_5\text{Gd}_{1-x}\text{Ca}_x) = x \cdot a(\text{Cu}_5\text{Ca}) + (1-x) \cdot a(\text{Cu}_5\text{Gd}) \quad (5)$$

where  $a$  denotes one of the hexagonal lattice parameters. Identical relation can be stated for lattice

parameter  $c$ . Experimental dependence of hexagonal lattice parameters on compositional factor  $x$  was found to be fairly linear, where the parameter  $a$  was increasing with Ca addition (Figure 5a), whereas parameter  $c$  was decreasing (Figure 5b). This is in good accordance with the formerly described Vegard's law for solid solutions, Eq. 5. Consequently, the unit cell volume, calculated as a volume of hexagonal prism (Eq. 6) was also increasing linearly with  $x$  (Figure 5c).

$$V = \frac{3\sqrt{3}}{2} a^2 c \quad (6)$$

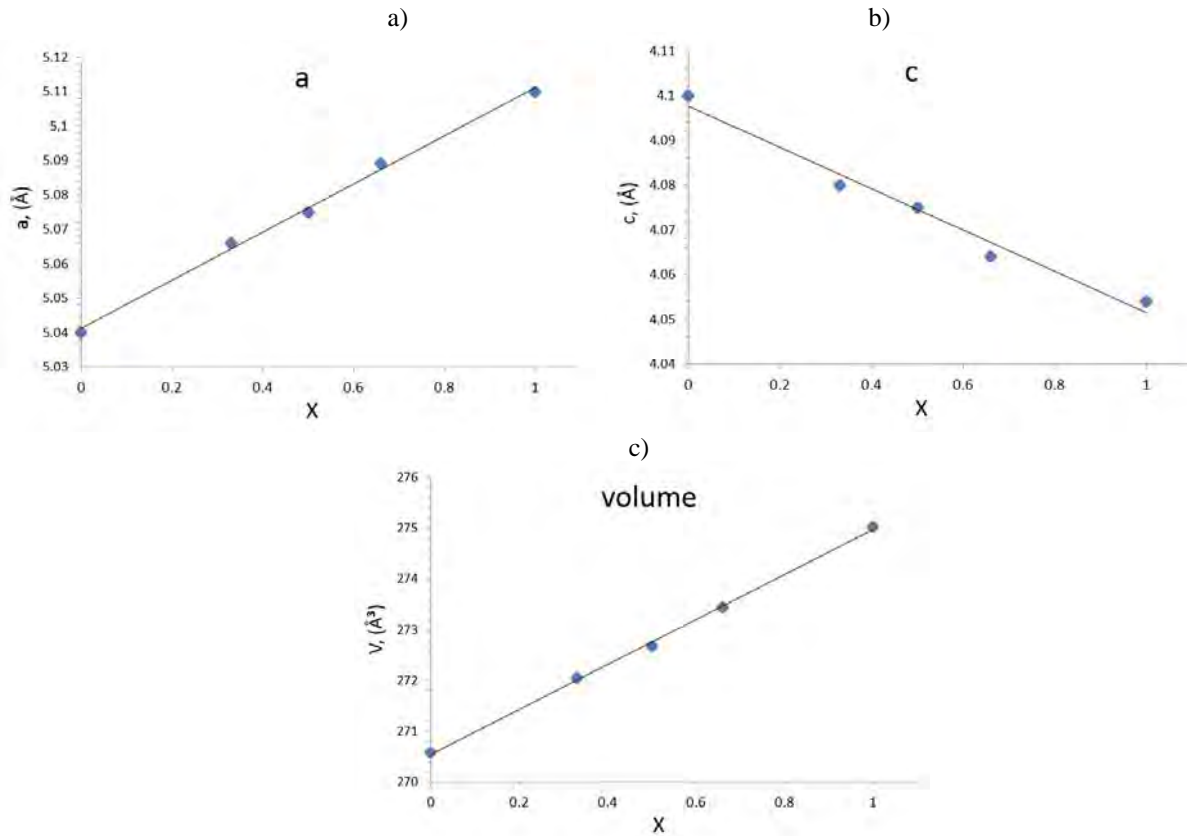


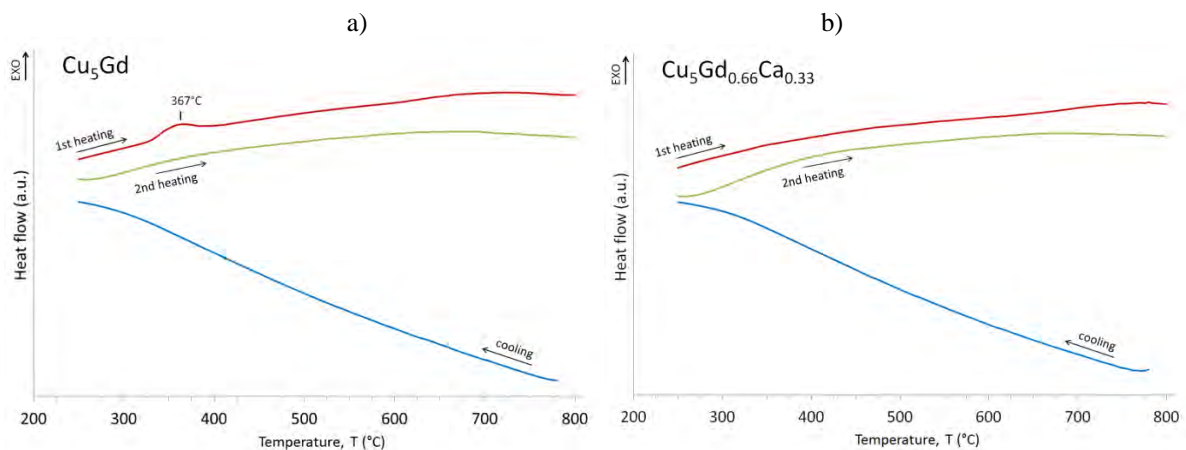
Figure 5. Plots of experimentally obtained lattice parameters  $a$  and  $c$  with respect to the compositional factor  $x$  in  $\text{Cu}_5\text{Gd}_{1-x}\text{Ca}_x$  system with corresponding unit cell volume. Linear fit serves as a guide for an eye.

#### Phase stability, DSC and HT XRD

In order to assess the stability of these rapidly solidified alloys, we performed DSC measurement as previously described, Figure 6. All the recorded peaks were irreversible, since none of them showed up upon cooling neither upon 2<sup>nd</sup> heating.  $x=0.33$  and  $0.5$  samples were considered as the most stable, since no DSC peaks were found, whereas all the rest contained low T exothermic signal, i.e.  $x=0.66$  and  $x=1$  at  $350^\circ\text{C}$  and  $x=0$  at  $367^\circ\text{C}$ . Due to the characteristic shape and irreversible nature of those peaks and the fact that the samples were rapidly solidified,

they could be attributed to the glass transition temperature.

Additionally, two endothermic DSC peaks were determined at  $560$  and  $660^\circ\text{C}$  for the two Ca-rich samples, i.e.  $x=0.66$  and  $x=1$ . For pure  $\text{Cu}_5\text{Ca}$ , the first peak was larger than for  $\text{Cu}_5\text{Gd}_{0.33}\text{Ca}_{0.66}$  and vice versa for the second peak. In order to check whether the hexagonal-to-cubic phase transition occurred, and which species formed at elevated temperatures in case of the Ca-rich samples, we performed high-temperature (HT) XRD analysis, Figure 7a–e, where the measurement temperatures were set upon the end of each DSC peak, i.e.  $400$ ,  $580$  and  $700^\circ\text{C}$ .



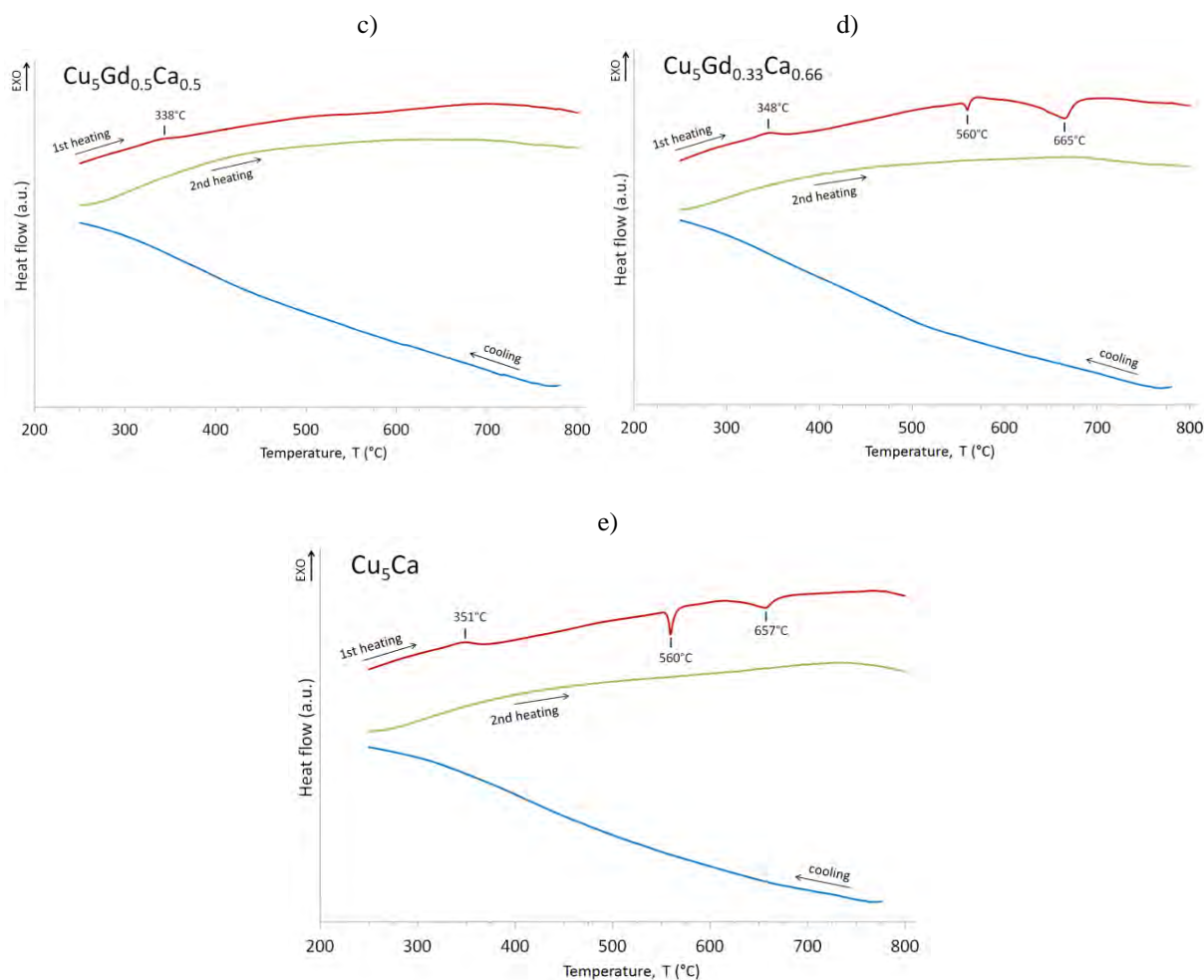


Figure 6. DSC analysis of  $\text{Cu}_5\text{Gd}_{1-x}\text{Ca}_x$  ( $x = 0, 0.33, 0.5, 0.66$  and  $1$ ) melt-spun ribbons during two-stage heating regime.

HT XRD data showed that diffraction peaks of stable cubic structure appeared already at  $400^\circ\text{C}$ , in all five investigated samples. Furthermore, the relative intensity of cubic phase got more pronounced as the temperature increased, which means that the hexagonal-to-cubic phase transition occurs over a large temperature interval, suggesting that it is of second order. Therefore, the DSC signal of this transition was smeared over wide temperature range and thus cannot be seen. Namely, when we compared HT XRD patterns of  $x = 0.33$  and  $x = 0.5$  samples with the rest, there was no significant difference – cubic structure formed in all cases. However, the DSC measurements of former implied no thermal events. For this reason, none of DSC signals observed in Figure 6 could be related to the hexagonal-to-cubic transformation. As previously described, DSC peaks at  $350$  and  $367^\circ\text{C}$  were due to the glass transi-

tion temperature, whereas to explain the  $560$  and  $660^\circ\text{C}$  endothermic peaks of the Ca-rich samples ( $x = 0.66$  and  $x = 1$ ) the HT XRD technique was insufficient, since no new phases appeared at those temperatures. Additionally, we noticed that in the case of  $\text{Cu}_5\text{Ca}$  sample hexagonal phase was still present at  $700^\circ\text{C}$ , which implies that hexagonal structure is the most stable when no gadolinium is present. Or, in other words, it is stabilized by calcium.

According to the Cu-Ca phase diagram and report of Chakrabarti et al. [13], we could attribute the  $560^\circ\text{C}$  peak to the following peritectic reaction:  $\beta\text{-CuCa} \leftrightarrow \text{Cu}_5\text{Ca} + \text{L}$ , which occurs at  $567^\circ\text{C}$ . The peak at  $660^\circ\text{C}$  was most likely due to the melting of aluminum, which formed upon reduction of alumina pot by segregated calcium metal.

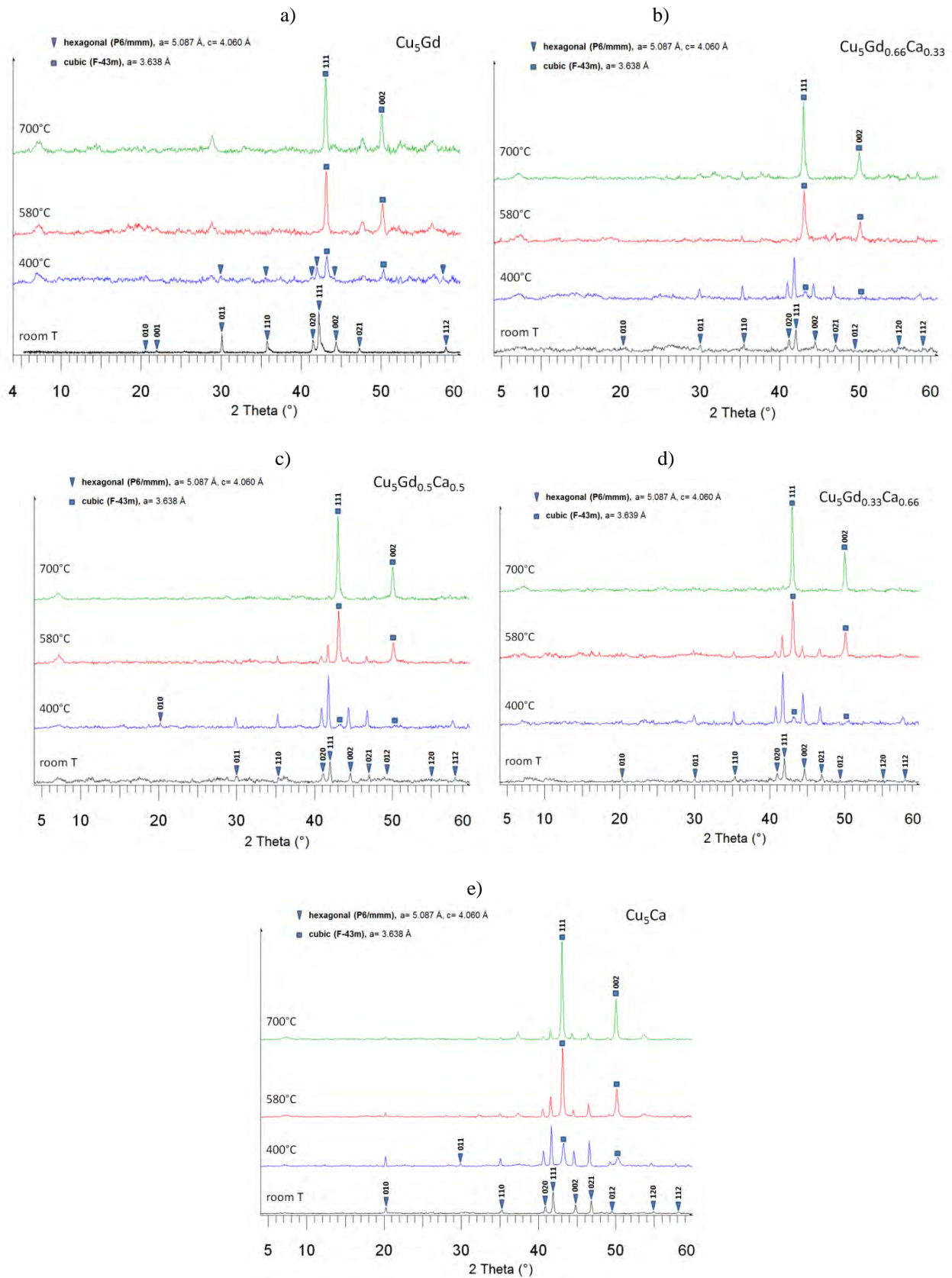


Figure 7a–e. High-temperature XRD patterns of  $\text{Cu}_5\text{Gd}_{1-x}\text{Ca}_x$  melt-spun ribbons recorded at room temperature, 400, 580 and 700°C; a)  $x = 0$ , b)  $x = 0.33$ , c)  $x = 0.5$ , d)  $x = 0.66$  and e)  $x = 1$ .

### Hydrogenation

After exposing the hexagonal as-spun samples to pure hydrogen atmosphere at 300°C for 16 hours, cubic (F-43m) hydrides formed, all containing approximately 0.5 wt. % of hydrogen. This is yet another proof that cubic structure of this particular system, either with or without hydrogen, is thermodynamically favorable over hexagonal phase. In fact, we believe that hydrogen accelerates this transformation via increased mobility of atoms. If not, hexagonal crystal lattice would solely expand

upon hydrogenation, which would appear as a shift of XRD peaks to lower angles. It is worth mentioning that Hruška et al. [21] reported on the following phase transition as the hydrogen concentration increases in bulk Gd:  $\alpha$  (hcp, Gd)  $\rightarrow$   $\beta$  (fcc,  $\text{GdH}_2$ )  $\rightarrow$   $\gamma$  (hcp,  $\text{GdH}_3$ ). Despite the fact that all hydrides had the same crystal structure, Figure 8a, the corresponding  $\text{H}_2$  mass-spectra, Figure 8b, were very different, which must be due to different chemical composition and consequently different hydrogen bonding energies (sites).

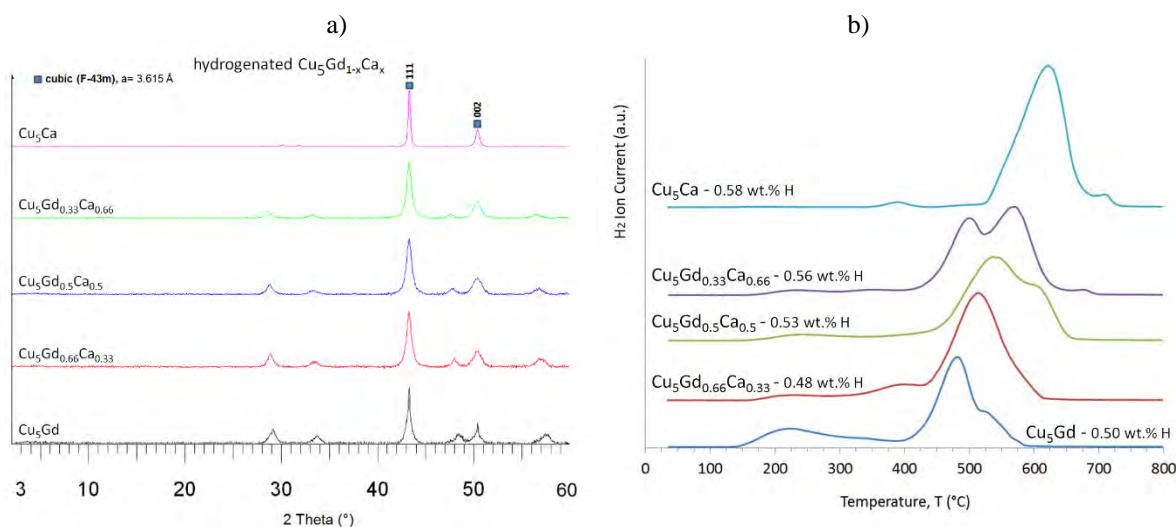


Figure 8. a) XRD patterns of hydrogenated  $\text{Cu}_5\text{Gd}_{1-x}\text{Ca}_x$  ( $x = 0, 0.33, 0.5, 0.66$  and  $1$ ) melt-spun ribbons, and b) corresponding mass-spectra of thermally desorbed hydrogen gas.

In general, when more calcium was in the alloy, higher temperatures were required for thermal hydrogen desorption, indicating that Ca-H has more negative formation enthalpy than Gd-H. Literature reports, however, show that gadolinium hydride ( $\text{Gd} + \text{H}_2 \rightarrow \text{GdH}_2$ ) has slightly more negative formation enthalpy than calcium hydride ( $\text{Ca} + \text{H}_2 \rightarrow \text{CaH}_2$ ), i.e.  $-196.3$  [22] and  $-181.5$  kJ/mol [23], respectively. Since copper hydride formation from gaseous hydrogen is viable only under severe pressure around 20 GPa [24], it does not promote hydrogen uptake in our samples.

In order to get the information about how Ca amount ( $x$ ) in the  $\text{Cu}_5\text{Gd}_{1-x}\text{Ca}_x$  system affects the interaction of protons with the host metallic lattice and find the correlation with Figure 8b, i.e. through proton diffusivity and hopping activation energies, we measured proton spin-lattice relaxation by means of nuclear magnetic resonance ( $^1\text{H}$  NMR). Proton hopping between the interstitial sites causes fluctuations in the inter-proton spin interactions and activation energy for these jumps can be obtained from the temperature dependence of proton spin-lattice relaxation time  $T_1$  [25]. However, it turned out that

proton  $T_1$  is roughly temperature-independent in the temperature range from room temperature to 120°C, where rapid proton hopping was expected. This indicated that the dynamic contribution to proton relaxation was masked by another contribution, perhaps due to proton coupling to paramagnetic centers in the sample (Gd), therefore no information about the activation energies for jumps could be obtained by  $^1\text{H}$  NMR.

#### Catalysis of oxygen reduction from gas phase

Another very interesting effect was observed during mass-spectrometry measurement of desorbed hydrogen. Namely, shortly after hydrogen gas was released from the samples, i.e. around 135°C for  $\text{Cu}_5\text{Gd}$ , there was an instantaneous and significant drop of oxygen ion current signal and a simultaneous jump of water signal, Figure 9. This was a strong evidence for the catalytic activity of these alloys for oxygen reduction reaction (ORR), though from gas phase. Oxygen was present as impurity and most probably came into the system from atmosphere through PE pipes for argon carrier gas.

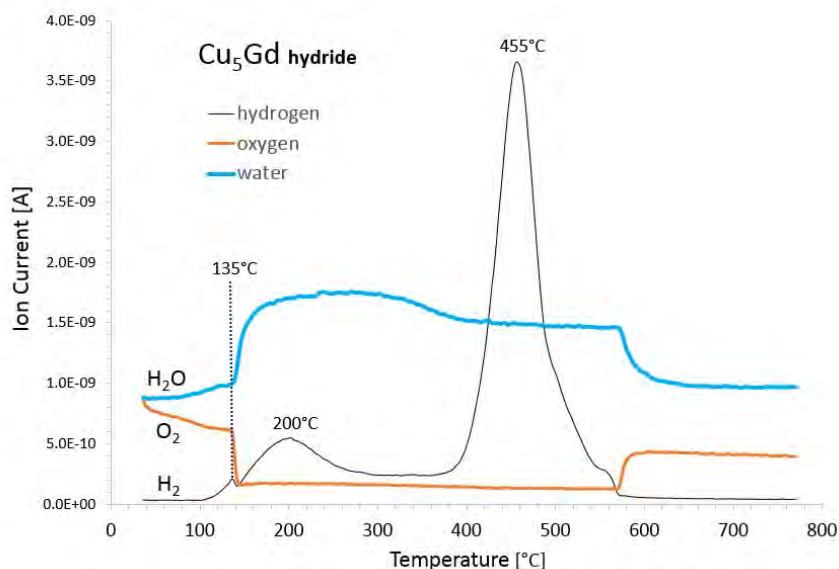


Figure 9. Signals of ionized species ( $\text{H}_2$ ,  $\text{O}_2$  and  $\text{H}_2\text{O}$ ) in quadrupole mass-spectrometer with respect to the temperature show high catalytic activity of hydrogenated  $\text{Cu}_5\text{Gd}$  alloy.

It is important to note that the reactant hydrogen gas came from the catalyst itself, which means that the reaction could occur at lower temperatures, if hydrogen (and oxygen) were delivered from external sources (gas cylinders). Thus, we performed such catalytic experiment, Figure 10, where in the first step we simulated the experiment from Figure 9, i.e. partial dehydrogenation in 5 %  $\text{O}_2/\text{He}$  mixture, which served as an activation step. After 20 min at  $200^\circ\text{C}$ , we switched off the oxygen source and cooled the sample down to  $40^\circ\text{C}$  in pure helium. Then, after 1 hour, we turned on the flow of stoichiometric mixture of  $\text{H}_2$  and  $\text{O}_2$  in argon and helium, respectively, so that the total concentration of hydrogen and oxygen in noble gases was around 5 vol. %. We observed instantaneous increase in water signal, already at  $40^\circ\text{C}$ , which then exponentially decreased for about 40% in 10 min and stayed constant until the sample temperature reached  $80^\circ\text{C}$ , where significant increasing of water signal was detected, reaching its maximum at  $207^\circ\text{C}$ . After 10 min, the signal again dropped for about 50%, though the temperature decreased only for  $5^\circ\text{C}$ . The first signal increase, when subjecting  $\text{Cu}_5\text{Gd}$  material to the mixture of hydrogen and oxygen at  $40^\circ\text{C}$ , is predominantly on account of shifting the process gas from neat He to the reactive mixture of  $\text{H}_2/\text{O}_2$  in inert gases. Catalytic activity was too minute to be visibly superimposed onto signal background. Nonetheless, upon linearly increasing the temperature, water formation ensued at the temperatures, lower than  $80^\circ\text{C}$ , resulting in a large catalytic water

formation peak at  $207^\circ\text{C}$ . The latter formation peak was verily mirrored by oxygen consumption downward peak at the corresponding temperatures. This strong boost in water production may be explained by the synergistic activity of both gaseous hydrogen (input stream) and the one at the topmost layers of the material, shifting the hydrogen content beyond stoichiometric, and thus increasing the rate of the catalyzed oxygen reduction and water formation. At some point, this readily available hydrogen from the material is depleted and the signal drops; nonetheless, some hydrogen is still trapped in the  $\text{Cu}_5\text{Gd}$  material and the surface hydrogen content boost now becomes dependent on the diffusion in the solid phase towards surface as the rate-determining step. After 120 min, the second peak decreases as well, and then, the resulting water formation activity may be ascribed solely to the catalytic transformation of the stoichiometric  $\text{H}_2/\text{O}_2$  mixture, causing about an order of magnitude higher water formation activity as compared to its analogue using neat oxygen mixture (e.g. at 25 min) or the  $\text{H}_2/\text{O}_2$  mixture at  $40^\circ\text{C}$  (105 min). This extrapolated difference in  $\text{H}_2\text{O}$  ion current signal between 40 and  $200^\circ\text{C}$  was denoted as  $\Delta\text{IC}(\text{H}_2\text{O})$ , in Figure 10, where its value for  $\text{Cu}_5\text{Gd}$  hydrogenated sample was found to be  $1.1 \cdot 10^{-9}$  A. The short-term stability tests exhibited no activity decrease for about 1 h of the exposure to reaction mixture; nevertheless, to obtain a more relevant benchmark, the tests would have to be prolonged to several days in more realistic environment (e.g. by adding impurities).

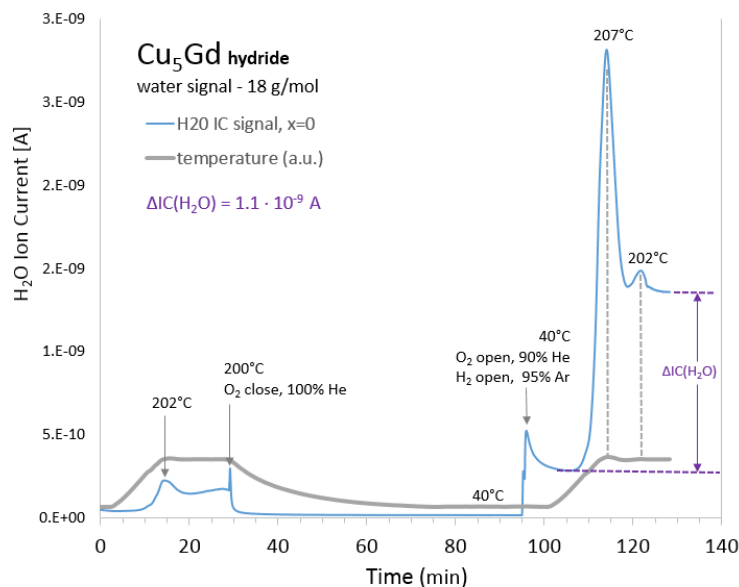


Figure 10. Two-step heating regime under controlled atmosphere yielded even higher catalytic activity of hydrogenated  $\text{Cu}_5\text{Gd}$  alloy, since water already formed at temperatures under  $80^\circ\text{C}$ .

In addition, we performed the same experiments for other investigated samples, where we found that calcium alters the catalytic activity, measured as  $\Delta\text{IC}(\text{H}_2\text{O})$ . Also, not hydrogenated, cubic  $\text{Cu}_5\text{Gd}$  was approximately 65% less active than its hydride counterpart. Such results can be explained through higher calcium oxidation affinity and absence of dehydrogenation and consequently activation in case of non-hydrogenated  $\text{Cu}_5\text{Gd}$ .

Further experiments should be made on these alloys to elucidate the origin of their catalytic activity for oxygen reduction from gas phase. It might be, however, related to cubic crystal structure, since as-spun hexagonal  $\text{Cu}_5\text{Gd}$  sample showed no activity. Another plausible explanation is regarded to copper segregation to the surface, where it oxidizes, and copper (II) oxide is very common catalyst for various oxidation reactions [26,27], including hydrogen oxidation [28]. However, this investigation is beyond the scope of the present work.

#### 4. CONCLUSION

We prepared a series of melt-spun ribbons by substitution of Gd with Ca in  $\text{Cu}_5\text{Gd}$  master alloy. After rapid quenching by melt-spinning, all samples exhibited hexagonal  $\text{P}_6/\text{mmm}$  structure regardless of Gd/Ca ratio, which implied on good substitutional solid solubility of Ca and Gd in the system with 83.3 at. % of Cu. Such finding was not surprising, since Carnasciali [10] and Subramanian [11] already reported that high temperature polymorph of  $\text{Cu}_5\text{Gd}$

compound has hexagonal  $\text{P}_6/\text{mmm}$   $\text{Cu}_5\text{Ca}$ -like structure ( $a = 5.04 \text{ \AA}$ ,  $c = 4.11 \text{ \AA}$ ). Thus, rapid quenching must be applied in order to fulfill the Hume-Rothery rule of the same crystal structure for solid solubility of two compounds, i.e.  $\text{Cu}_5\text{Gd}$  and  $\text{Cu}_5\text{Ca}$ . Namely, at slow cooling  $\text{Cu}_5\text{Gd}$  crystallizes in low temperature cubic F-43m,  $\text{AuBe}_5$ -like modification, which apparently is not compatible with hexagonal structure of  $\text{Cu}_5\text{Ca}$  and thus strong phase separation occurs at slow cooling. It seems that this Hume-Rothery condition is required for solid solution formation beside thermodynamics, i.e. enthalpy and entropy of mixing, as described in the Introduction chapter.

However, by XRD no secondary phases could be identified in as-spun  $\text{Cu}_5\text{Gd}_{0.5}\text{Ca}_{0.5}$  ribbons, whereas TEM revealed presence of Cu-Ca precipitates within predominant matrix phase, thus both phases must have the same crystal structure. By HT XRD and DSC, we confirmed that hexagonal phase of all investigated samples is metastable, as second order phase transition into stable cubic structure occurred upon heating. In the case of  $\text{Cu}_5\text{Ca}$  binary alloy residual hexagonal peaks were still present at  $700^\circ\text{C}$ , which indicates that hexagonal structure is stabilized by calcium. Also, hydrogen induced hexagonal-to-cubic phase transition at  $300^\circ\text{C}$ , where all hydride samples had the same structure, whereas there was a substantial difference in their hydrogen mass-spectra, indicating on severely modified electronic structure upon Gd substitution with Ca.

The discovery of high catalytic activity of  $\text{Cu}_5\text{Gd}$  sample for water formation from gaseous hydrogen and oxygen represents great challenge to

perform further work on this material in order to understand the nature of its catalytic activity and to test it for other chemical reactions and potential technological applications, i.e. PEM fuel cells, car exhaust systems, etc., where expensive Pt is used nowadays.

## 5. ACKNOWLEDGEMENTS

This research was part of the bilateral French-Slovenian PROTEUS project CalGad-X. Authors are grateful to Dr. Marjeta Maček for assistance at DSC and mass-spectrometry experiments, and to Ms. Urška Kavčič for catalytic tests under controlled atmosphere, funded by Slovenian National Research Program P2-0152.

## 6. REFERENCES

- [1] R. W. Cahn, P. Hassen, North Holland, Amsterdam, 1996, vol. 1.
- [2] A. Takeuchi, A. Inoue, *Quantitative evaluation of critical cooling rate for metallic glasses*, Mater. Sci. Eng. A, Vol. 304–306 (2001) 446–451.
- [3] Y. Zhang, Y. J. Zhou, J. P. Lin, G. L. Chen, P. K. Liaw, *Solid solution phase formation rules for multi-component alloys*, Adv. Eng. Mater., Vol. 10 (2008) 534–538.
- [4] S. Guo, C. Ng, J. Lu, C.T. Liu, *Effect of valence electron concentration on stability of fccor bcc phase in high entropy alloys*, Journal of Applied Physics, Vol. 109 (2011) 103505–103510.
- [5] S. Guo, Q. Hu, C. Ng, C.T. Liu, *More than entropyalloys:forming solid solutions or amorphous phase*, Intermetallics, Vol. 41 (2013) 96–103.
- [6] C. A. Gearhart, *Einstein before 1905: the early papers on statistical mechanics*, American Journal of Physics, Vol. 58–5 (1990) 468–480.
- [7] Y. Zhang, T. T. Zuo, Z. Tang, M. C. Gao, K. A. Dahmen, P. K. Liaw, Z. P. Lu, *Microstructures and properties of high-entropy alloys*, Progress in Materials Science, Vol. 61 (2014) 1–93.
- [8] A. R. Ruffa, *Thermal potential, mechanical instability, and melting entropy*, Physical Review B, Vol. 25–9 (1982) 5895–5900.
- [9] H. Okamoto, *Desk Handbook: Phase Diagrams for binary alloys*, 2<sup>nd</sup> Edition, ASM International, 2010.
- [10] M. M. Carnasciali, S. Cirafici, E. Franceschi, *On the Gd-Cu system*, Journal of the Less-Common Metals, Vol. 92 (1983) 143–147.
- [11] P. R. Subramanian, D. E. Laughlin, *The Cu-Gd (Copper-Gadolinium) System*, Bulletin of Alloy Phase Diagrams, Vol. 9–3a (1988) 347–354.
- [12] F. Merlo, M. L. Fornasini, *The Structures of  $\alpha$ -CaCu,  $\beta$ -CaCu, SrAg and BaAg: Four Different Stacking Variants Based on Noble-Metal-Centered Trigonal Prisms*, Acta Crystallographica, Vol. B37 (1981) 500–503.
- [13] D. J. Chakrabarti, D. E. Laughlin, *The Ca-Cu (Calcium-Copper) System*, Bulletin of Alloy Phase Diagrams, Vol. 5–6 (1984) 570–576.
- [14] H. Kato, M. I. Copeland, *USBM-U-952*, Metallurgical Progress Rep., No. 15, National Technical Information Service, Springfield, VA (1962).
- [15] K. A. Gschneider, Jr. and F. W. Calderwood, *Ca-Gd (Calcium-Gadolinium)*, Bulletin of Alloy Phase Diagrams, 8(6), Dec 1987.
- [16] A. Inoue, A. P. Tsai, T. Masumoto, *Stable decagonal and icosahedral quasicrystals*, Journal of Non-Crystalline solids, Vol. 117–118, Part 2 (1990) 824–827.
- [17] Y. Luo, A. Habrioux, L. Calvillo, G. Granozzi, N. Alonso-Vante, *Thermally induced strains on the catalytic activity and stability of Pt–M<sub>2</sub>O<sub>3</sub>/C (M = Y or Gd) catalysts towards oxygen reduction reaction*, ChemCatChem, Vol. 7 (2015) 1573–1582.
- [18] Y. Luo, A. Habrioux, L. Calvillo, G. Granozzi, N. Alonso-Vante, *Yttrium oxide/gadolinium oxide-modified platinum nanoparticles as cathodes for the oxygen reduction reaction*, ChemPhysChem, Vol. 15 (2014) 2136.
- [19] I. Chorkendorff, *Understanding the new class of Pt<sub>3</sub>X, and Pt<sub>5</sub>X (X = Sc, Y, La and Gd) oxygen reduction catalysts and their activation mechanism*, Abstr. Pap. Am. Chem. S., Vol. 245 (2013) 463-ENFL.
- [20] A. R. Denton, N. W. Ashcroft, *Vegard's law*, Phys. Rev. A, Vol. 43–6 (1991) 3161–3164.
- [21] P. Hruška, J. Čížek, P. Dobroň, W. Anwand, A. Mücklich, R. Gemma, S. Wagner, H. Uchida, A. Pundt, *Investigation of nanocrystalline Gd films loaded with hydrogen*, Journal of Alloys and Compounds, Vol. 645–1 (2015) S308–S311.
- [22] G. E. Sturdy, R. N. R. Mulford, *The Gadolinium-Hydrogen System*, Journal of the American Chemical Society, Vol. 78–6 (1956) 1083–1087.
- [23] P. Rittmeyer, U. Wietelmann, *Hydrides*, Ullmann's Encyclopedia of Industrial Chemistry, Wiley-VCH, Weinheim, (2002), doi: 10.1002/14356007.a13 199.
- [24] C. Donnerer, T. Scheler, E. Gregoryanz, *High-pressure synthesis of noble metal hydrides*,

The Journal of Chemical Physics, Vol. 138 (2013) 134507.

[25] A. Gradišek, T. Apih, *Hydrogen dynamics in partially quasicrystalline Zr<sub>69.5</sub>Cu<sub>12</sub>Ni<sub>11</sub>Al<sub>7.5</sub>: A fast field-cycling relaxometric study*, The Journal of Physical Chemistry C, Vol. 119–19 (2015) 10677–10681.

[26] M. Shimokawabe, H. Asakawa, N. Takezawa, *Characterization of copper/zirconia*

*catalysts prepared by an impregnation method*, Applied Catalysis, Vol. 59–1 (1990) 45–58.

[27] Lj. Kundaković, M. Flytzani-Stephanopoulos, *Reduction characteristics of copper oxide in cerium and zirconium oxide systems*, Applied Catalysis A: General, Vol. 171–1 (1998) 13–29.

[28] R. N. Pease, H. S. Taylor, *The reduction of copper oxide by hydrogen*, Journal of American Chemical Society, Vol. 43–10 (1921) 2179–2188.



### ТОПЉИВОСТ ЧВРСТИХ ТВАРИ У СИСТЕМУ Cu<sub>5</sub>Gd<sub>1-x</sub>Ca<sub>x</sub> : СТРУКТУРА, СТАБИЛНОСТ, ХИДРОГЕНАЦИЈА И КАТАЛИЗА РЕДУКЦИЈЕ КИСЕОНИКА

**Сажетак:** Проучавали смо ефекте замјене гадолинијума у смјеси Cu<sub>5</sub>Gd са Са испитујући фазну стабилност и кристалну структуру насталих нових смјеса. За рапидно хлађене материјале произведене завртањем талине, кристална структура је увијек била хексагонална P<sub>6</sub>/mmm, без обзира на додавање Са (x) у смјесама са формулом Cu<sub>5</sub>Gd<sub>1-x</sub>Ca<sub>x</sub>, индицирајући добру топљивост чврстог тијела под оваквим условима, што је додатно потврђено Вегардовим законом. Спорије хлађење након процеса лучног топљења узроковало је фазну сепарацију у Cu<sub>4</sub>Gd и CuСа. Користећи ТЕМ, испитали смо рапидно очврснуте траке од Cu<sub>5</sub>Gd<sub>0.5</sub>Са<sub>0.5</sub> и посматрали заједничко дјеловање Cu–Са секундарне фазе са фазом матрице која има номинални стохиометријски састав. Ниво кисеоника у овом узорку је био у оквиру 2–5 ат. %, што је приписано површинској оксидацији током или након припреме ТЕМ узорка. Након хидрогенације, кристална структура свих узорака се промијенила из хексагоналне у кубну (F-43m), што је термодинамички стабилан полиморф Cu<sub>5</sub>Gd смјесе. Јака каталитичка активност стварања воде од гасовитог H<sub>2</sub> и O<sub>2</sub> је случајно откривена током експеримента дехидрогенације, тиме чинећи овај материјал потенцијалним кандидатом за нулто-платински катализатор редукције кисеоника.

**Кључне ријечи:** брза солидификација, топљивост чврстих твари, фазни пренос, хидрогенација, катализа.

